Title

Adhesion and Surface Interactions of a Self-Healing Polymer with Multiple Hydrogen-Bonding Groups

Journal

Advanced Functional Materials, 24(16)

ISSN

1616-301X

Authors

Faghihnejad, Ali
Feldman, Kathleen E
Yu, Jing
et al.

Publication Date

2014-04-01

DOI

10.1002/adfm.201303013

ADVANCED FUNCTIONAL MATERIALS
www.afm-journal.de

Adhesion and Surface Interactions of a Self-Healing Polymer with Multiple Hydrogen-Bonding Groups

*Ali Faghihnejad, Kathleen E. Feldman, Jing Yu, Matthew V. Tirrell, Jacob N. Israelachvili, Craig J. Hawker, Edward J. Kramer, and Hongbo Zeng**

The surface properties and self-adhesion mechanism of self-healing poly(butyl acrylate) (PBA) copolymers containing comonomers with 2-ureido-4[1H]-pyrimidinone quadruple hydrogen bonding groups (UPy) are investigated using a surface forces apparatus (SFA) coupled with a top-view optical microscope. The surface energies of PBA–UPy4.0 and PBA–UPy7.2 (with mole percentages of UPy 4.0% and 7.2%, respectively) are estimated to be 45–56 mJ m^{-2} under dry condition by contact angle measurements using a three probe liquid method and also by contact and adhesion mechanics tests, as compared to the reported literature value of 31–34 mJ m^{-2} for PBA, an increase that is attributed to the strong UPy–UPy H-bonding interactions. The adhesion strengths of PBA–UPy polymers depend on the UPy content, contact time, temperature and humidity level. Fractured PBA–UPy films can fully recover their self-adhesion strength to 40, 81, and 100% in 10 s, 3 h, and 50 h, respectively, under almost zero external load. The fracture patterns (i.e., viscous fingers and highly "self-organized" parallel stripe patterns) have implications for fabricating patterned surfaces in materials science and nanotechnology. These results provide new insights into the fundamental understanding of adhesive mechanisms of multiple hydrogen-bonding polymers and development of novel self-healing and stimuli-responsive materials.

1. Introduction

The field of supramolecular chemistry utilizes multiple, reversible, and in certain cases, cooperative intermolecular interactions to create new materials with unique properties and functionalities. The non-covalent intermolecular interactions typically utilized in the design of supramolecular materials and polymers include hydrophobic,[1,2] hydrogen bonding,[3–8] metal-ligand,[9–11] and ionic interactions.[12] Over the last two decades many synthesis strategies have been developed to design new supramolecular polymers with unique characteristics such as enhanced bulk properties (i.e., plateau modulus, tensile modulus), self-healing capability, stimulus-responsiveness and the ability to assemble into well-defined nanostructures.[5–7,9,13–19] Self-healing polymer materials or composites have attracted considerable attention over the past decade due to their controllable and reversible molecular interactions, interesting mechanical properties and potential applications.[5,18] Many conventional healing approaches used in thermoplastic polymers and thermoset composites such as microencapsulation and thermally reversible crosslinks (covalent bonds) require treatments at high temperature (i.e., high energy input). Another widely used method for developing self-healing polymers is by incorporating strong and reversible non-covalent hydrogen bonding moieties into the polymer structure. For example, the 2-ureido-4[1*H*]-pyrimidinone (UPy) group is a strong quadruple-hydrogen-bonding dimer which was first used by Sijbesma et al.[3] to synthesize supramolecular polymers, and has been shown to be highly thermally responsive.[20,21]

A. Faghihnejad, Prof. H. Zeng
Department of Chemical and Materials Engineering
University of Alberta
Edmonton, AB, T6G 2V4, Canada
E-mail: hongbo.zeng@ualberta.ca
Dr. K. E. Feldman, Prof. J. N. Israelachvili,
Prof. C. J. Hawker, Prof. E. J. Kramer
Materials Department
University of California
Santa Barbara, CA 93106, USA
Dr. K. E. Feldman, Prof. J. N. Israelachvili,
Prof. C. J. Hawker, Prof. E. J. Kramer
Materials Research Laboratory
University of California
Santa Barbara, CA 93106, USA
Dr. J. Yu, Prof. J. N. Israelachvili, Prof. E. J. Kramer
Department of Chemical Engineering
University of California
Santa Barbara, CA 93106, USA
Prof. M. V. Tirrell
Institute for Molecular Engineering
University of Chicago
Chicago, IL 60637, USA
Prof. C. J. Hawker
Department of Chemistry and Biochemistry
University of California
Santa Barbara, CA 93106, USA

DOI: 10.1002/adfm.201303013

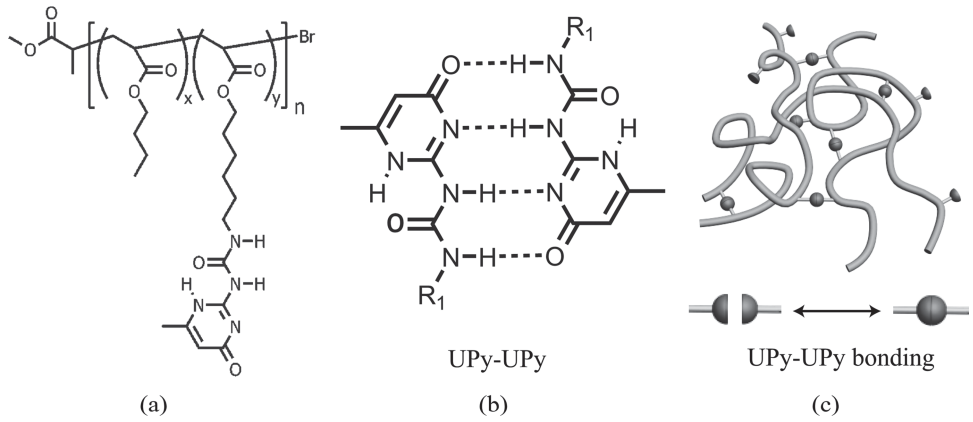

Figure 1. Schematics of a) the chemical structure of P(nBA-*r*-UPy), b) hydrogen bonds between two UPy groups, and c) polymer chains functionalized with UPy groups.

In addition, the properties and applications of supramolecular materials are largely determined by the strength of the non-covalent (adhesion) interactions and the interaction kinetics. As a result, understanding the various factors governing the formation of non-covalent bonds and the effects of environment conditions is crucial for the development of advanced functional supramolecular materials. Despite the progress in the development and characterization of supramolecular polymers with various chemical structures, understanding their molecular and surface interaction mechanisms remains limited.

In the present work the surface properties and adhesion mechanisms of a supramolecular self-healing polymer, UPy-functionalized poly(*n*-butyl-acrylate) were investigated by using a surface forces apparatus (SFA) as well as the complementary techniques of atomic force microscopy (AFM), optical microscopy, and contact angle goniometry. An SFA coupled with a top-view optical microscope, which has been previously used in the studies of adhesion and friction mechanisms of various polymer surfaces as well as molecular interactions of both biological and non-biological systems,[22–30] was employed to study the contact mechanics and adhesion between self-healing UPy-functionalized poly(*n*-butyl-acrylate) films. The surface deformations and patterns associated with the adhesion and detachment of these supramolecular polymer films were monitored in situ in real time through multiple beam interferometry (MBI) in the SFA as well as the top-view optical microscope, followed by further examination with AFM. Since UPy groups are capable of forming multiple hydrogen bonds, we also investigated the effects of UPy monomer content of the polymers and different environmental conditions such as the relative humidity and temperature on the adhesion and contact behaviour of the polymer surfaces. The self-healing capability of UPy functionalized polymer during adhesion and detachment cycles was also investigated. The surface interaction mechanisms and potential applications of the self-healing polymer will be discussed.

2. Materials and Methods

Random copolymers of *n*-butyl acrylate backbones with quadruple hydrogen-bonding side chains of 2-ureido-4[1*H*]-pyrimidinone (UPy), Poly (*n*-butyl acrylate-*r*-UPy acrylate), or P(nBA-*r*-UPy), were synthesized and characterized as reported previously.[7] Schematics of the chemical structure of P(nBA-*r*-UPy) and hydrogen bonding between two UPy groups are shown in **Figure 1**.

Copolymer solutions were prepared by dissolving the polymers in toluene (Fisher Scientific, Canada, high-performance liquid chromatography (HPLC) grade, 99.9%) that were filtered using 0.2 μm filters before use. P(nBA-*r*-UPy) with repeat units functionalized with two different mole percentages of UPy were studied in this work: 4.0% UPy and 7.2% UPy, denoted by PBA–UPy4.0 and PBA–UPy7.2, respectively, with molecular weights M_n of 24.8 and 25.3 kg mol^{-1}, and polydispersities of ≈1.3.[7] Polymer films were prepared by spin coating of 0.5 wt% polymer solution on mica or silica substrates, and stored overnight (>12 h) in vacuum to remove the solvent and leave a uniform smooth film of thickness ≈100 nm. The polymer surfaces were then mounted into the SFA chamber in a crossed-cylinder geometry (each cylinder of radius R = 2 cm), which is equivalent to the interaction between a sphere of radius R and a flat surface, or between two spheres of radius 2R, when the surface separation D is much smaller than R ($D << R$). The polymer film thickness in each case was measured using multiple beam interferometry (MBI) in the SFA by using fringes of equal chromatic order (FECO), and confirmed by ellipsometry.[31]

X-ray photoelectron spectroscopy (XPS) and contact angle measurements were also conducted to characterize the properties of the polymer surfaces. The contact angles of three probe liquids of known surface tensions (water, ethylene glycol and diiodomethane) on the polymer films were measured using a Ramé-Hart contact angle goniometer to estimate the surface energies of the P(nBA-*r*-UPyA) polymers based on the method developed by van Oss et al.[32]

An SFA was used to investigate the adhesion and contact mechanics of the polymer films under different conditions. Details of the SFA experimental setup have been reported previously.[33–35] A top-view optical microscope was coupled with the SFA, as reported previously,[25–27,36] to observe the surface patterns associated with the adhesion and detachment of the polymer films. The SFA experiments were performed at two relative humidities (RH) of RH = 0% (dry condition) and

RH = 100% (saturated water vapour condition) and two different temperatures of T = 23 °C (room temperature) and T = 40 °C. The temperature of the SFA chamber was increased by inserting two heating rods into the walls of the SFA and the temperature was monitored by a thermistor. The surfaces were mounted in the SFA chamber one hour prior to each experiment in order to reach equilibrium under the desired temperature and humidity level. At each experimental condition at least two pairs of polymer surfaces were tested in SFA and for each pair at least three different positions were examined to confirm the reproducibility of the data. The surface features of the adhesive junctions of the polymer films after the adhesion tests were characterized by an optical microscope (Axioskop 40, Carl Zeiss, Germany) and an atomic force microscope (Asylum, MFP-3D-Bio, Santa Barbara, CA, USA).

3. Results and Discussion

3.1. Characterization of the Polymer Thin Films and Their Surfaces

Typical AFM images of PBA–UPy4.0 and PBA–UPy7.2 thin films in dry air and after exposure to humid air for 1 h are shown in Figure S1 (Supporting Information). Figure S1 shows that both polymer films are smooth, with rms roughnesses of 0.3 nm and 0.2 nm for PBA–UPy4.0 and PBA–UPy7.2 films, respectively, and that relative humidity does not have a significant effect on the morphology of the films at room temperature. The XPS spectra of nitrogen (N1s) for the two types of polymer films are shown in Figure S2 (Supporting Information). The nitrogen peak intensity is proportional to the amount of the UPy groups present on the polymer surface. As expected, Figure S2 confirms that higher amount of UPy groups are present on PBA–UPy7.2 surface than polymer PBA–UPy4.0.

The contact angles of three probe liquids (i.e., ethylene glycol, diiodomethane and water) on the polymer surfaces as a function of time are shown in **Figure 2**. The surface energy of the polymers was determined using the method developed by van Oss et al.[32] as follows. In general, when a droplet of liquid **2** forms a contact angle θ on a surface of material **1** in medium **3**, the interfacial energies are related by Young's equation:

$$\gamma_{12} + \gamma_{23}\cos\theta = \gamma_{13} \quad (1)$$

If medium **3** is air, Equation 1 reduces to

$$\gamma_{12} + \gamma_2\cos\theta = \gamma_1 \quad (2)$$

According to the van Oss method the surface energy is comprised of two terms which take into account the contributions from Lifshitz–van der Waals (γ^{LW}) and Lewis acid-base (γ^{AB}) interactions as

$$\gamma = \gamma^{LW} + \gamma^{AB} \quad (3)$$

The Lewis acid-base component of the surface energy is defined such that it comprises the electron-acceptor and electron-donor interactions given by

$$\gamma^{AB} = 2\sqrt{\gamma^+\gamma^-} \quad (4)$$

Based on Equations 3,4, Young's equation can be written as

$$\gamma_2(\cos\theta + 1) = 2\left(\sqrt{\gamma_1^{LW}\gamma_2^{LW}} + \sqrt{\gamma_1^+\gamma_2^-} + \sqrt{\gamma_1^-\gamma_2^+}\right) \quad (5)$$

By measuring the contact angle of three probe liquids and using the above equations, one can determine the Lifshitz–van der Waals and the acid-base components of the surface energy of polymers.[37,38] The initial values at t = 0 of the contact angles in Figure 2 were used in the calculations of the surface energies of the PBA–UPy polymers. The surface energies γ of the polymers as estimated from the contact angle measurements and the above equations are summarized in **Table 1**. From Table 1, the surface energies of PBA–UPy4.0 and PBA–UPy7.2 were estimated to be γ = 51 and 57 mJ m^{-2}, respectively, which are much higher than the reported value of γ = 33.7 mJ m^{-2} for non-functionalized poly(*n*-butyl-acrylate) (PBA) at 20 °C.[39] The enhanced surface energy of PBA–UPy is mainly due to the effect of hydrogen bonding among the UPy groups in increasing the polar contributions of the surface energy, as shown in Table 1: γ^{AB} = 11 and 17 mJ m^{-2} for PBA–UPy4.0 and PBA–UPy7.2, respectively. It was also found that the presence of UPy groups in PBA could dramatically increase its glass transition temperature and the T_g of PBA–UPy4.0 and PBA–UPy7.2 are 11 °C and 22 °C higher than non-functionalized PBA, respectively.[7] Previous experiments have shown that carboxylated PBA with 5 mol% of –COOH groups almost has the same T_g as non-functionalized PBA.[40] These results demonstrate that the multiple hydrogen-bonding group UPy can enhance the intermolecular interactions (or cohesion) between the polymer chains more drastically than simple polar functional group (e.g., carboxylic group), thus significantly enhancing the surface energy.

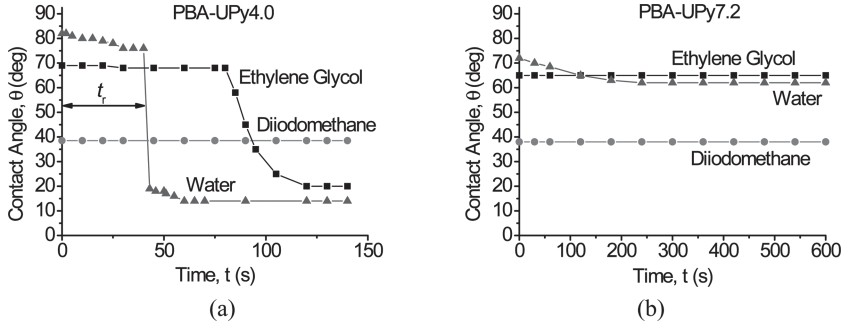

Figure 2. Contact angles of three liquids on the polymer films of a) PBA–UPy4.0 and b) PBA–UPy7.2 of thickness 120 nm vs time, t. PBA–UPy4.0 film became ruptured after contacting with water for time t_r, so-called rupture time.

Figure 2a shows that the water contact angle on polymer PBA–UPy4.0 surface first dropped from 82° to 76° in $t_r \approx 40$ s and then dropped abruptly which was coupled with the rupture of the thin polymer film. Similar rupture behavior occurred for ethylene glycol on PBA–UPy4.0 film after $t_r \approx 85$ s. The typical rupture patterns are shown in Figure S3 (Supporting Information). The effect of film thickness on the rupture time t_r and

Table 1. Surface energy components of the three probe liquids[69] and the two polymers PBA–UPy4.0 and PBA–UPy7.2 in (mJ m^{-2}) estimated from the initial contact angles (Figure 2) using Equation 1 to 5.

Material	γ	γ^{LW}	γ^{AB}	γ^{+}	γ^{-}
Diiodomethane	50.8	50.8	≈ 0	≈ 0.01	≈ 0
Ethylene glycol	48	29	19	3.0	30.1
Water	72.8	21.8	51	25.5	25.5
Polymer PBA–UPy4.0	51	40	11	2	15
Polymer PBA–UPy7.2	57	40	17	3	27
Polymer PBA	33.7[39]	–	–	–	–

the possible rupture mechanism are discussed in Figures S4,S5 (Supporting Information). Figure 2b shows that contact angles of the three probe liquids were stable on the polymer PBA–UPy7.2 surface and only the water contact angle slightly decreases from 72° to 62° after ≈5 min. The facts that contact angle of non-polar diiodomethane remains constant and water contact angle decreases ($t < t_r$, before rupture) indicate that the hydrogen bonding between water molecules and the UPy groups in PBA–UPy could be enhanced with time which most likely leads to the reconstruction of the polymer surface leading to an increase in the areal density of UPy segments there. The above speculations could be further supported by the increased γ values (γ = 57 and 69 mJ m^{-2} for PBA–UPy4.0 and PBA–UPy7.2, respectively) as estimated by using the decreased water contact angles.

3.2. Contact and Adhesion Mechanics of Polymer Thin Films: Effects of Relative Humidity, Temperature and Time

Contact mechanics tests[22,41] were conducted to investigate the adhesion of the PBA–UPy4.0 and PBA–UPy7.2 films at T = 23 and 40 °C. The classical theory of contact mechanics of surfaces was first studied by Hertz in 1888[42] and followed by Johnson, Kendall and Roberts (JKR model), Derjaguin, Muller and Toporov (DMT model), and Maugis.[43–45] In general for soft materials of large radius with high surface energy (e.g., polymers) the JKR model is more applicable, while for hard materials of low surface energy and small radius of curvature the DMT model is more appropriate.[38,41] According to the JKR model, for two elastic surfaces with surface energy γ under an external load $F_\perp$, the radius of the contact area a is given by

$$a^3 = \frac{R}{K}\left(F_\perp + 6\pi R\gamma + \sqrt{12\pi R\gamma F_\perp + (6\pi R\gamma)^2}\right) \quad (6)$$

where R is the radius of an elastic sphere pressed against a flat surface which is equivalent to two perpendicular cylinders of radius R based on Derjaguin approximation, K is the equivalent modulus, related to Young's moduli E and the Poisson ratios ν by $K = 2E/3(1 - \nu^2)$.[29] The corresponding adhesion or pull-off force is given by

$$F_\perp^{ad} = 3\pi R\gamma \quad (7)$$

The contact diameter $2a$ as a function of applied load $F_\perp$ during loading and unloading of PBA–UPy4.0 and PBA–UPy7.2 at T = 23 and 40 °C under two different relative humidity levels of RH = 0% and RH = 100% are shown in **Figure** 3a–d. The adhesion forces (or pull-off forces) and corresponding effective surface energies γ_{eff} ($=F_\perp^{ad}/3\pi R$)[24,38] are summarized in Figure 3e. The loading and unloading rates were $k_\perp V_\perp$ = 0.3 mN s^{-1} and $k_\perp$ is the stiffness of the force measuring spring (corresponding to separation velocity $V_\perp$ = 0.33 μm s^{-1}). The waiting time at the maximum load $F_{\perp,max}$ ≈ 33 mN was fixed at 15 s.

As shown in Figure 3, hysteresis was observed for the loading and unloading paths under all the conditions tested above, and both relative humidity and temperature show significant impact on the adhesion behavior of both copolymers. For example, at T = 23 °C and RH = 0%, the adhesion for PBA–UPy4.0 and PBA–UPy7.2 were $F_\perp^{ad}$ ≈ 33 and 38 mN, corresponding to γ_{eff} = 170 and 202 mJ m^{-2} as shown in Figure 3a,e. When the relative humidity was increased to RH = 100% at T = 23 °C, the adhesion forces increased to $F_\perp^{ad}$ ≈ 49 and 57 mN, corresponding to γ_{eff} = 260 and 302 mJ m^{-2} respectively, as shown in Figure 3b,e.

Although significant adhesion hysteresis was measured during unloading, the contact behavior during loading of the PBA–UPy polymers still roughly follows the predictions of the JKR model, as shown by the solid lines in Figure 3 and also reported for other polymer systems.[22,24,25,38,46] The fitted surface energies of the two polymers on loading under different experimental conditions are tabulated in **Table 2**. In general, the surface energies in Table 2 were close to the values in Table 1 that were calculated based on the initial contact angles measurements, for example: PBA–UPy4.0 (JKR vs contact angle method: γ ≈ 45 vs 51 mJ m^{-2}) and PBA–UPy7.2 (γ ≈ 49 vs 57 mJ m^{-2}) at room temperature. The difference between the values obtained from the two methods could be due to several possible factors: the selection of probe liquids in contact angle measurements, and the partial elastic nature of the polymers. As the polymers become liquid-like, the presence of UPy groups plays a smaller role in the adhesion, and the surface energy values are closer to the value γ_0 for poly(n-butyl acrylate) of γ_0 ≈ 31–34 mJ m^{-2}.[39,47]

A higher adhesion force was measured for PBA–UPy7.2 than PBA–UPy4.0 for almost all the above cases (except at RH = 100% and T = 40 °C, discussed later), which is attributed to the higher amount of UPy groups for the PBA–UPy7.2 chains and at the polymer/dry air interface as confirmed by XPS (see supporting information). The UPy groups at the opposing polymer surfaces could form multiple hydrogen bonds during contact, enhancing the polymer adhesion. Exposing the polymer films to air at 100% relative humidity for one hour could increase the density of UPy functional groups on the polymer surfaces and led to an increase in the adhesion force. It is noted that the water contact angle on polymer PBA–UPy7.2 decreased by about 10 degrees after a few minutes due to the overturning or migration of polar UPy groups at the polymer surface. Recent theoretical analysis shows that UPy–UPy binding energy can be reduced from ≈–161 kJ mol^{-1} in vacuum to –69 kJ mol^{-1} in water and that the binding energy of interaction between UPy and water molecules is competitive with that of UPy-UPy.[48] Temperature also has a significant impact on the self-adhesion

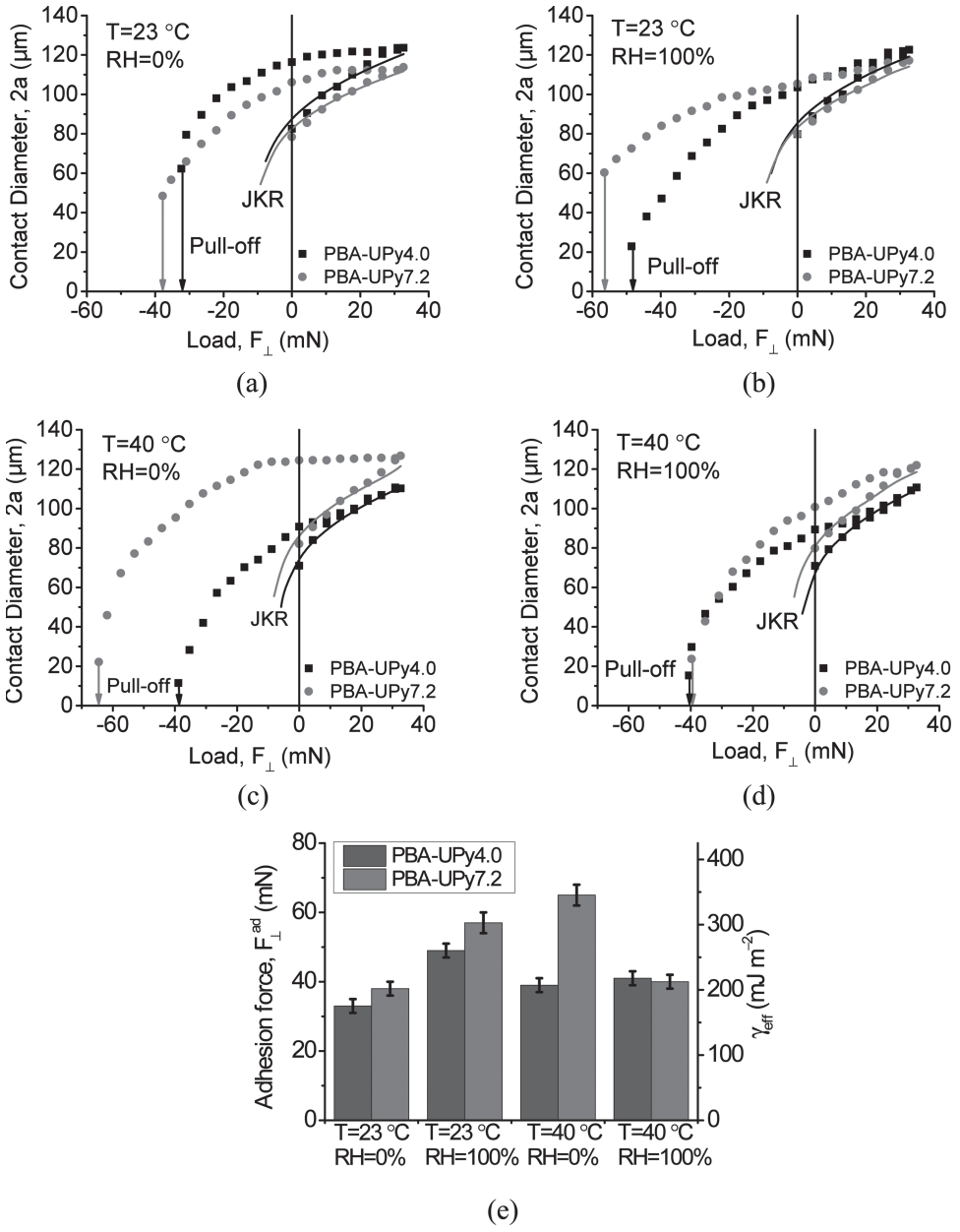

Figure 3. Contact diameter vs applied load for a,c) PBA–UPy4.0, b,d) PBA–UPy7.2 polymer films (thickness ≈ 100 nm) at a,b) room temperature (T = 23 °C) and c,d) T = 40 °C and two relative humidity levels of RH = 0% and RH = 100%. e) Summary of adhesion forces and effective surface energies of PBA–UPy polymers at different experiment conditions. Loading and unloading rates were $k_{\perp}V_{\perp}$ = 0.3 mN s^{-1} or $V_{\perp}$ = 0.33 μm s^{-1}, and waiting time at the maximum load $F_{\perp,max}$ = 33 mN was 15 s.

Table 2. Surface energies of polymers PBA–UPy4.0 and PBA–UPy7.2 in mJ m^{-2} estimated from JKR fitting of the loading curves in contact mechanics tests (Figure 3).

Polymer	T = 23 °C		T = 40 °C	
	RH = 0%	RH = 100%	RH = 0%	RH = 100%
PBA–UPy4.0	45 ± 3	42 ± 2	31 ± 3	26 ± 3
PBA–UPy7.2	49 ± 2	50 ± 3	43 ± 3	36 ± 2

of PBA–UPy polymers. Increasing T = 23 °C to 40 °C at RH = 0% leads to an increase in the adhesion forces for both PBA–UPy4.0 and PBA–UPy7.1, which is attributed to enhanced interpenetration of polymer chains across the contact interface at 40 °C as a result of increased mobility of polymer chains.[22–24]

The above results show that the adhesion of PBA–UPy4.0 and PBA–UPy7.2 are affected mainly by the viscoelastic properties of the polymer films, the surface density of UPy groups, as well as the degree of interpenetration of polymer chains across the contact interface and temperature, rate and time (discussed

later). The experimental temperatures were higher than the glass transition temperatures of PBA–UPy4.0 and PBA–UPy7.2, and the adhesion hysteresis and the contact behaviors (as also discussed later) indicate that both polymers behave viscoelastically.[7] As the relative humidity increases, water molecules interact with the free UPy functional groups on the polymer surface, and may also diffuse into the bulk of the polymer film, thus changing both the surface energy and the viscoelastic properties of polymer film, which is supported by the contact mechanics data of PBA–UPy4.0 at RH = 0% and 100%, T = 23 °C, as shown in Figure 3a,b (viz. the contact diameter right before pull-off was much smaller at RH = 100% compared to that at RH = 0%, therefore the polymer film was more liquid-like). It should be noted that the water-UPy interaction has to compete with the UPy–UPy interaction which involves four hydrogen bonds (see Figure 1). For the PBA–UPy7.2 polymer, its higher T_g, longer effective bond lifetime τ_b^* (≈3 vs ≈20 s),[7] lower mobility of its chains and a stronger interaction due to the increased mole fraction of UPy groups make the PBA–UPy7.2 polymer more elastic[7] than the PBA–UPy4.0 polymer and the diffusion of water molecules in the PBA–UPy7.2 film would be relatively more difficult than that for the PBA–UPy4.0 case.[49–53] Increasing the relative humidity also dramatically increases the density of free UPy functional groups on the surface,[48] and this effect is relatively more significant for PBA–Upy7.2 than for PBA–UPy4.0. The overall effect of relative humidity on the bulk viscoelastic properties (e.g., G′, G″) and surface chemistry (γ values) of the two PBA–UPy polymers, is to increase their adhesion by ≈50% when increasing the relative humidity from 0% to 100% at room temperature.

As shown in Figure 3e, on increasing the temperature from 23 to 40 °C at RH = 0%, the adhesion of PBA–UPy4.0 and PBA–UPy7.2 increased by ≈20% and ≈70%, respectively. Increasing the relatively humidity further to 100% at 40 °C has almost no effect on the adhesion of PBA–UPy4.0 while it decreases the adhesion of PBA–UPy7.2 to be the same value as PBA–UPy4.0. These results suggests that for PBA–UPy4.0, the UPy-UPy hydrogen bonds can easily form and break at 40 °C, and that the bulk properties dominate the polymer adhesion—the polymer essentially behaves like a viscous liquid, which was further supported by the viscous fingering phenomena associated with the detachment process (discussed later). For PBA–UPy7.2, increasing the temperature from 23 to 40 °C at RH = 0% leads to further increased interpenetration of polymer chains at the contact interface and allows formation of multiple UPy-UPy bonds across the interface. As a consequence, PBA–UPy7.2 still behaves like a soft elastic solid as supported by the contact behavior (enhanced adhesion) and fracture patterns associated with the adhesion tests (discussed later). When the relative humidity was further increased to 100% at 40 °C, PBA–UPy7.2 now behaves more like a viscous liquid, and viscous fingering patterns were observed during the detachment process (discussed later).

It was observed that the contact time also plays an important role in the adhesion of the PBA–UPy polymers. To investigate the effect of total contact time, t_c, defined as the total time from first contact to final detachment, the polymer surfaces were kept in contact at the maximum load ($F_{\perp,max}$≈ 33 mN) for different times before separation. The effect of total contact time and unloading rate on the measured adhesion of PBA–UPy4.0 and PBA–UPy7.2 at room temperature is shown in **Figure 4**. The corresponding adhesion force is converted to the effective surface energy γ_{eff} by Equation 7.[24,38,46] Figure 4 shows that the effective adhesion of both PBA–UPy4.0 and PBA–UPy7.2 increase dramatically with t_c as

$$\gamma_{eff} \propto F_{\perp}^{ad} \propto t_c^n \tag{8}$$

where n = 0.13 ± 0.01 and 0.18 ± 0.01 for PBA–UPy4.0 and PBA–UPy7.2, respectively. The increase of the adhesion with total contact time is mainly due to the formation of more UPy-UPy H-bonds (Figure 1) across the interface with time. As expected, the higher density of UPy groups on the PBA–UPy7.2 surfaces lead to a faster increase of the adhesion with contact time compared to PBA–UPy4.0, as shown in Figure 4. It is interesting to note in Figure 4a,b that with increasing contact time, the contact area (πa^2) remained constant during the initial stage of separation. The constant contact area phenomenon was more pronounced for PBA–UPy7.2 at long contact times (t_c > 2 h), shown in Figure 4b; the contact area only decreased at high negative loads close to detachment.

If the surfaces are kept in contact for a sufficiently long time the two surfaces totally coalesce and the contact interface is expected to "disappear". In this limit we expect tensile failure to occur and the tensile failure strength would be obtained. For example when $t_c \approx 2.5 \times 10^5$ s, $F_{\perp}^{ad} \approx 130$ mN, $\gamma_{eff} \approx 700$ mJ m^{-2}, and the contact diameter $2a \approx 120$ μm, so that the tensile strength of the submicroscopic adhesive junction (or confined thin film) of PBA–UPy7.2 can be estimated to be at least $\sigma_c = F_{\perp}^{ad}/\pi a^2 \approx 11$ MPa. Similarly, the minimum tensile strength of the submicroscopic adhesive junction of PBA–UPy4.0 is estimated to be $\sigma_c \approx 4.8$ MPa. These tensile strengths (for the submicroscopic adhesive junctions of thickness ~200 nm) are much higher than reported values for the bulk tensile failure strengths of PBA–UPy polymers in the dogbone geometry (specimens of width ≈1 cm and thickness ≈0.2 cm),[54] which gave ≈1.7 MPa and <0.5 MPa for PBA–UPy7.2 and PBA–UPy4.0, respectively. The results here on the enhanced tensile failure strengths of confined thin film of multiple hydrogen-bonded PBA–UPy polymers are consistent with our recent report on confined submicroscopic thin films of glassy polystyrene.[28]

The effect of unloading rate on the adhesion force and the corresponding effective surface energy is shown in Figure 4d, in which the surfaces were kept in contact under $F_{\perp,max} \approx 33$ mN for 240 s. Figure 4d shows that with decreasing the unloading rate from $V_{\perp} \approx 0.33$ to ≈ 0.004 μm s^{-1} the adhesion force almost keeps constant for PBA–UPy4.0 while it slightly increases for PBA–UPy 7.2. The adhesion measured largely depends on the UPy–UPy H-bond life time,[7] debonding rate (related to the unloading rate), and enhanced surface density of UPy groups at the contact interface (related to the total contact time). It should be noted that during the measurements of Figure 4d, the total contact time t_c was actually different under the distinct unloading rates (the slower the unloading rate, the longer the total contact time). Therefore, the different trends measured between PBA–UPy4.0 and PBA–UPy 7.2 in Figure 4d are mainly attributed to the change in total contact time. Nevertheless, the effective surface energies measured in Figure 4d are

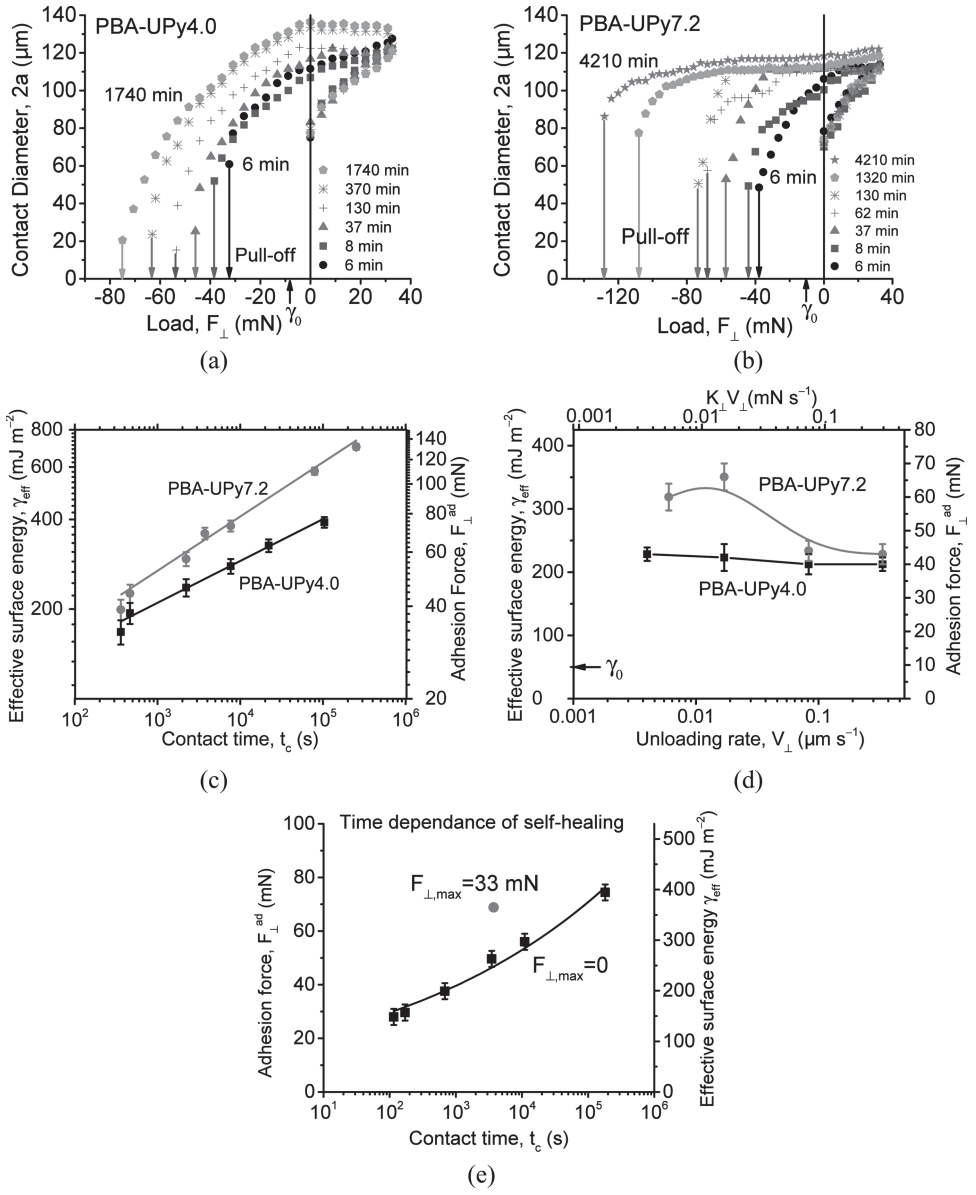

Figure 4. Contact diameter vs external load during JKR tests under different contact time for a) PBA–UPy4.0 and b) PBA–UPy7.2 polymer films of thickness ≈100 nm at room temperature, c) the adhesion force measured vs total contact time, and d) the adhesion force vs unloading rate. Note that the unloading rate was $k_{\perp}V_{\perp} = 0.3$ mN s^{-1} or $V_{\perp} = 0.33$ μm s^{-1} for (a–c). e) The effect of total contact time on the self-healing adhesion between two PBA–UPy7.2 films of thickness 107 nm under zero pre-loading condition ($F_{\perp,max} = 0$). The red data point shows the initial adhesion of the polymer films (for $F_{\perp,max} = 33$ mN and $t_c \approx 3700$ s).

much higher than the thermodynamic equilibrium value γ_0, which indicates that a much lower unloading rate would be needed to measure γ_0.

In summary, the contact and adhesion mechanics measurements of the two PBA–UPy polymer films show that their adhesive properties are determined by the surface density of H-bonding groups/segments that can interpenetrate across the contacting interface, and the bulk viscoelasticity of the polymer that determines its viscous forces, consistent with previous studies on polymer-polymer adhesion of uncrosslinked homopolymers.[22,24,38,46] The presence of UPy functional groups can dramatically enhance the polymer adhesion mainly due to the formation of multiple hydrogen bonds across the contact interface. The adhesion of PBA–UPy polymers can be significantly affected by temperature, humidity, unloading rate and contact time.

3.3. Self-Healing of Multiple Hydrogen-Bonding PBA–UPy Polymer

One of the more interesting aspects of multiple hydrogen-bonding polymers is their self-healing properties. The self-healing ability of PBA–UPy7.2 was investigated as follows: two

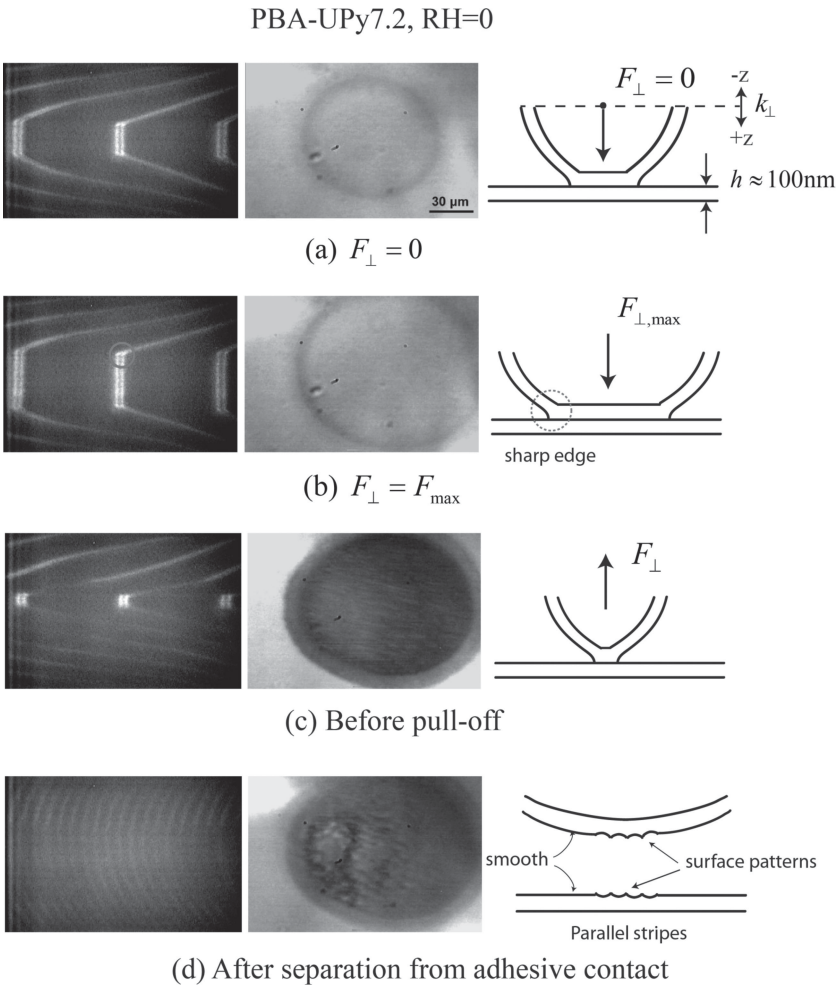

Figure 5. FECO fringe patterns (left), corresponding top-view optical microscope images (middle) and illustrations (right) of the contact junction of PBA–UPy7.2 polymer of thickness 100 nm at $T = 40$ °C and RH = 0%. Illustration in (a) shows that one surface is supported by a force measuring spring with stiffness $k_\perp$ which can drive the surface close to or away from the opposing surface.

previously fractured films of the polymer were brought back into contact for different contact times at RH = 0%. Each set of self-healing experiments was conducted at the same fractured position of the polymer films. The adhesion recovery of the surfaces under different contact times is shown in Figure 4e with the initial measured adhesion (under $F_{\perp,\max} = 33$ mN and $t_c \approx 3700$ s) shown by the red data point. Figure 4e shows that the adhesion recovered to more than 40% of the original value in ≈10 s (viz., the time for surfaces in contact before separation), and to ≈81% in 3 h, and continued to recover with time, reaching ≈108% of the original adhesion after ≈50 h of contact. It should be noted that the self-healing tests in Figure 4e were all under zero external load (viz., the force measuring spring was brought to the same position as the zero load condition for the first measurement,[34] as illustrated in **Figure 5**a). It is also noted that the self-healing process could be further expedited under a finite external load which presumably enhances the intimate contact of the two fractured surfaces.[5] The adhesion results in Figure 4e indicate that PBA–UPy polymer has excellent self-healing ability, which is mainly attributed to the reversible multiple hydrogen bonding of opposing UPy groups between PBA–UPy surfaces.

3.4. Characterization of Surface Patterns Associated with Adhesion Tests

As mentioned earlier, various types of surface deformations and patterns were observed during the adhesion tests of viscoelastic PBA–UPy polymers. Classic theories of contact and adhesion mechanics deal with the adhesion of two purely elastic materials and are static (equilibrium) models that describe the mechanical equilibrium states of the materials in contact. The adhesion of viscous and viscoelastic materials involves the dynamic growth of the adhesive junction and transient surface patterns during adhesive contact or "coalescence" as well as during detachment that cannot be described by classic theories. Molecular diffusion (interpenetration) across the interface alters the adhesion energy with time, which is also not included in the JKR theory that assumes $\gamma =$ constant. Experimental and theoretical works have been conducted on the contact and adhesion dynamics of viscoelastic and viscous materials and polymers to study these complex transient patterns, although a unified theory is still not available.[24–28,55–62]

The FECO patterns and corresponding top-view optical microscope images during four different stages in contact mechanics experiments of PBA–UPy7.2 at T = 40 °C and RH = 0 and 100% are shown in **Figure** 5 and **6**, respectively: a) the instant after the polymer surfaces came into adhesive contact ($F_\perp = 0$), b) contact under the maximum compressive load ($F_\perp = F_{\max}$), c) the instant just before pull-off or detachment, and d) after detachment. We may note the sharp contact edge in the FECO patterns in Figure 5b compared to the "rounded" (or meniscus-like) contact edge in Figure 6b (see the red circles) which indicates that the PBA–UPy7.2 film is more elastic at $T = 40$ °C and RH = 0% (Figure 5b) while it is more viscous and liquid-like at $T = 40$ °C and RH = 100% (Figure 6b). The discontinuity of the contact edge observed in the even fringe of the FECO fringes in Figure 6a,b indicates formation of a meniscus during the coalescence of the two PBA–UPy7.2 films.[24,63] The top-view images in Figure 6 further show the surface deformation at the contact boundary (interface between air and polymer neck), which is evident of the formation of transient fingering patters associated with coalescence/detachment of viscous polymer films, as reported recently.[25–27]

Interesting radial or randomly oriented parallel bands or stripe patterns (Figure 5c,d) and viscous fingering patterns (Figure 6c,d) were observed during the separation of

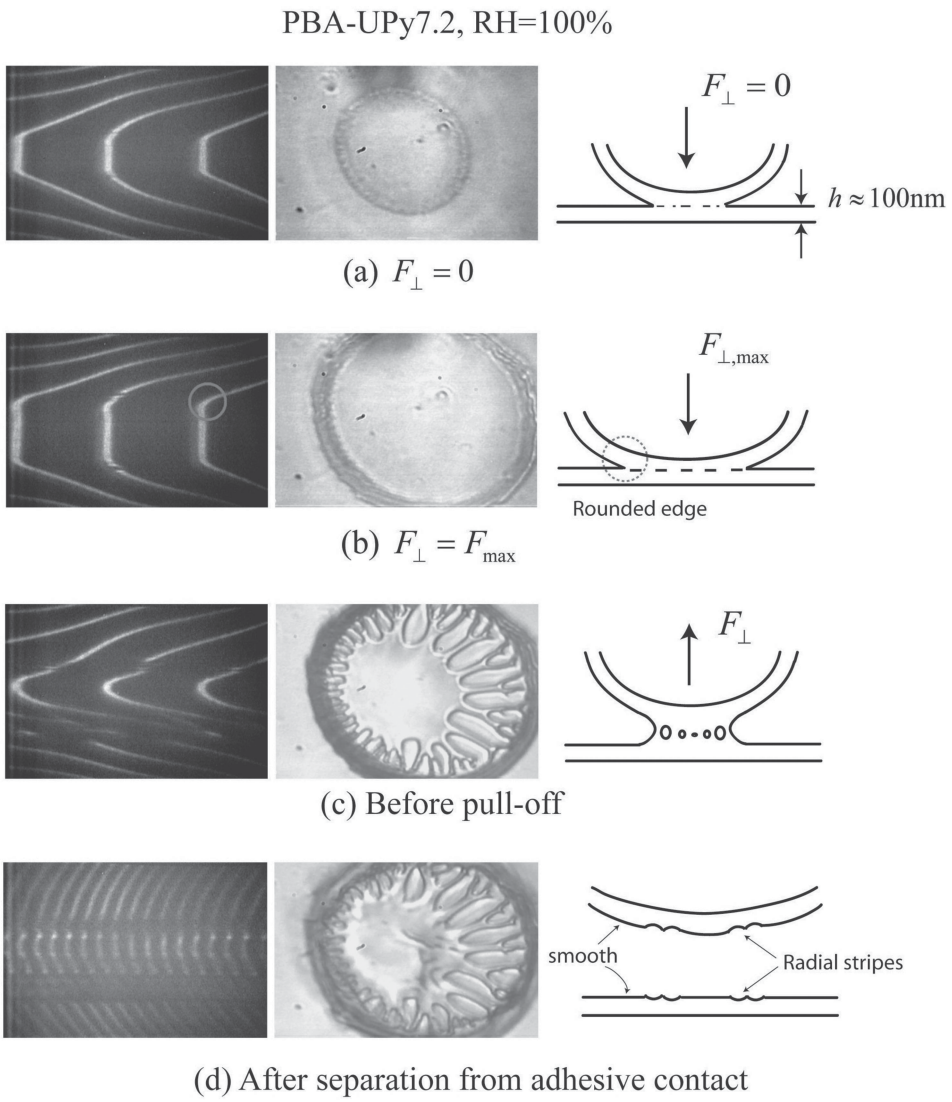

Figure 6. FECO fringe patterns (left), corresponding top-view optical microscope images (middle) and illustrations (right) of the contact junction of PBA–UPy7.2 polymer of thickness 100 nm at T = 40 °C and RH = 100%.

PBA–UPy7.2 at T = 40 °C, RH = 0 and 100%. It is evident from the fingering instability patterns observed at RH = 100% that the polymer becomes less elastically and more viscous as the relative humidity increases which supports the results of Figure 3d.

The surfaces were further characterized after the contact mechanics experiments. **Figure** 7 and Figure S6 (Supporting Information) show AFM images and optical microscopy images of typical surface deformation patterns associated with detachment of PBA–UPy7.2 films at T = 40 °C, RH = 0% and RH = 100%. As clearly shown in Figure 7, the surface patterns are significantly different as the relative humidity changes. At RH = 0% the surface patterns are in the form of linear and almost parallel bands or stripes while at RH = 100% much larger branched radial fingers are developed. Similar fracture patterns were reported previously for polystyrene in which linear parallel fractures and radial fingering instabilities were developed for elastic and viscous films, respectively.[24,25,28,64] Therefore PBA–UPy7.2 undergoes a transition from elastic to viscous failure or rupture as the relative humidity increases from RH = 0% to RH = 100% at T = 40 °C, which corroborates our results and discussion in the previous sections.

Figure 7a shows that for PBA–UPy7.2 at RH = 100% and T = 40 °C, the viscous fingers have a typical wavelength of λ = 9 ± 1 μm with a height amplitude of about 200–300 nm. Similar fingering instabilities were previously observed during the separation of confined viscous or viscoelastic films which was attributed to a mechanism involving Saffman-Taylor (fingering) instabilities.[24,26,28,65], According to Saffman–Taylor theory[66] when a high viscous fluid is displaced by a low viscous fluid in a confined geometry, viscous fingers with wavelength greater than λ_c can occur, where λ_c is given by

$$\lambda_c = 2\pi h\sqrt{\gamma/12V(\eta_1 - \eta_2)} \quad (9)$$

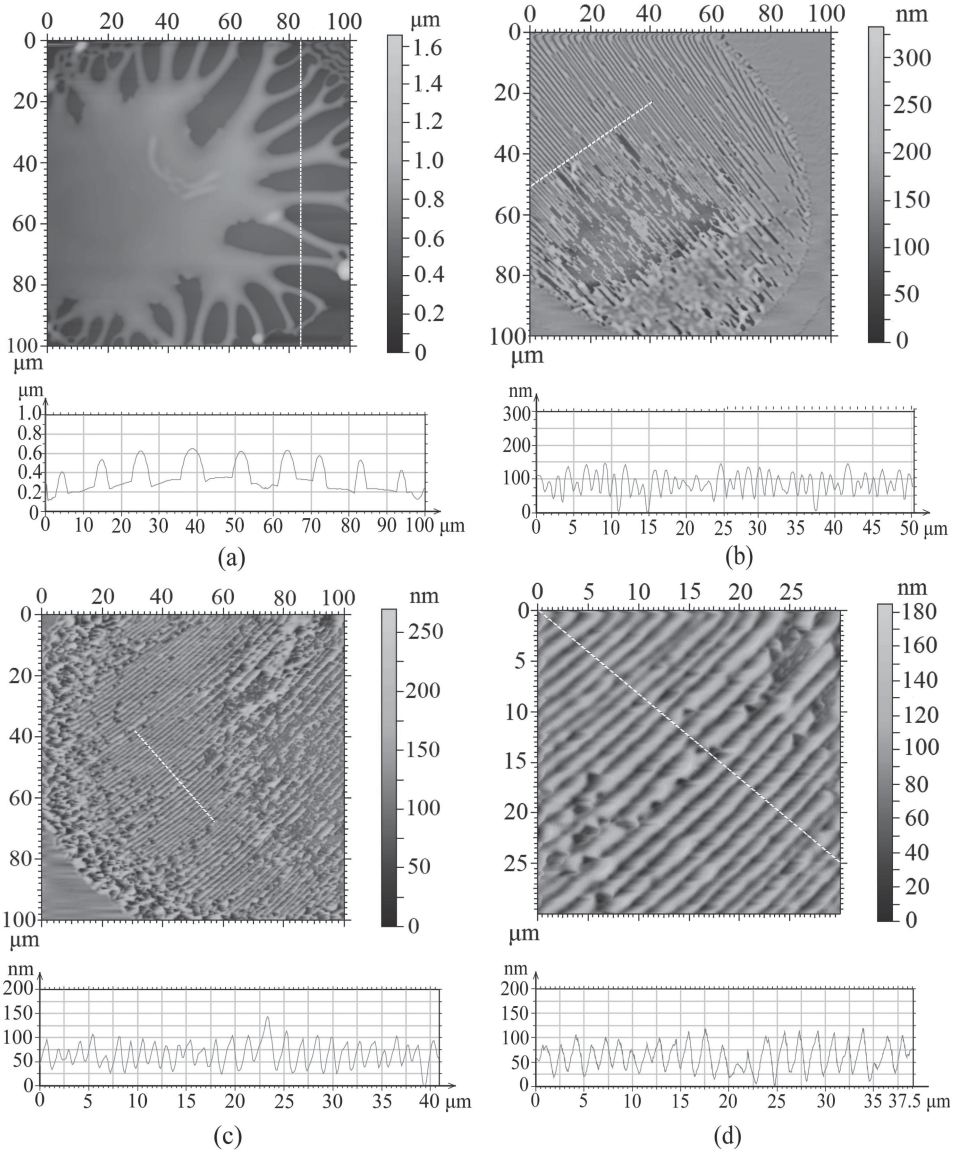

Figure 7. Typical topographical AFM images of surface patterns associated with the detachment of two PBA–UPy7.2 films (of thickness ≈ 100 nm) from adhesive contact in contact mechanics tests: a) more viscous state, RH = 100%, b–d) more elastic state, RH = 0%. The experiment temperature was T = 40 °C.

where h is the gap height or confined film thickness (in SFA experiments), γ is the interfacial tension, V is the velocity of the moving interface, and η_1, η_2 are the viscosities of polymer and air, respectively. Using some typical values before detachment in experiments: $h \approx 200$ nm, $\gamma \approx 36$ mJ m^{-2} (see Table 2), $V \approx 0.2$–5 μm s^{-1}, $\eta_2 \approx 0$, and $\eta_1 \approx 10^3$ Pa s at 40 °C and RH = 100%, Equation 9 yields $\lambda_c \approx$ 1–5 μm which is consistent with the experimental observation in Figure 7a.

In contrast, Figure 7b–d shows that the surface patterns for PBA–UPy7.2 at T = 40 °C and RH = 0% are parallel bands with typical wavelength of $\lambda \approx 1$ μm and height amplitude of about 80–100 nm. Several previous studies on deformation of confined soft elastic films showed that instability patterns are different from those of viscous films described by Saffman–Taylor theory. Recent studies[25,28,65,67,68] show that the wavelength of elastic instabilities are given by $\lambda \propto \pi h\sqrt{\gamma/Eb}$, where E is the elastic modulus of the polymer film and h is the confined film thickness; and it was also found that the wavelength λ depends on confined film thickness h according to $\lambda \approx (2.0 - 4.5)\,h$ and is independent of the crack propagation velocity. Therefore, putting $h \approx 200$ nm yields $\lambda \approx 900$ nm, which agrees well with the experimental value of $\lambda \approx 1$ μm shown in Figure 7b–d. It should be noted that similar parallel stripe patterns were also observed for PBA–UPy4.0 and PBA–UPy7.2 at T = 23 °C and RH = 0%, indicating that the copolymers is more elastic under these conditions.

The highly self-organized surface patterns associated with the contact mechanics tests of multiple hydrogen-bonded PBA–UPy polymer films show important implications in fabricating patterned surfaces with various applications

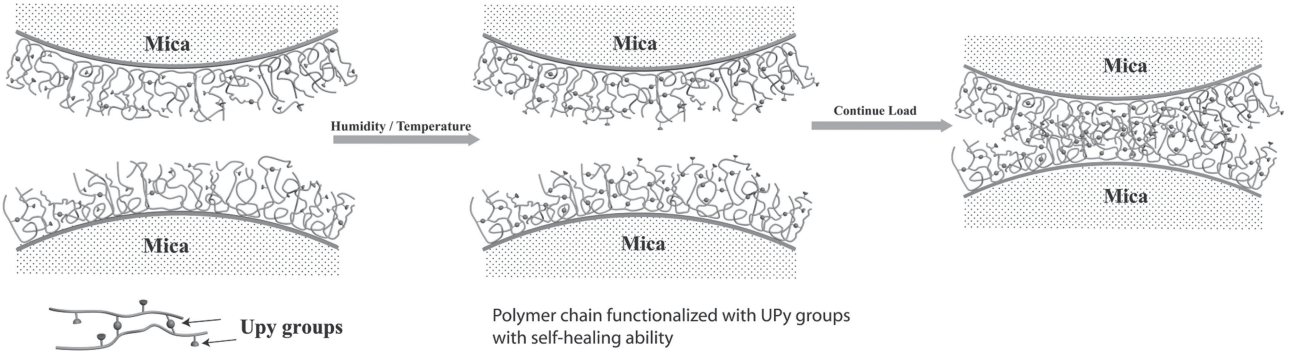

Figure 8. Schematic of the adhesion mechanisms of multiple hydrogen-bonding polymers.

such as microfluidic devices, display, sensors and smart surfaces.[25,28,64]

4. Conclusions

The surface characteristics and adhesion properties of a self-healing polymer with quadruple hydrogen bonding UPy groups, PBA–UPy, were investigated using different complementary techniques. The surface energies of PBA–UPy4.0 and PBA–UPy7.2 were estimated to be 45–56 mJ m^{-2} under dry conditions by contact angle measurements using a three probe liquid method and also by contact and adhesion mechanics tests, which depend on the UPy content, temperature and relative humidity. These surface energies are somewhat higher than the reported literature value of $\gamma \approx$ 31–34 mJ m^{-2} for poly (n-butyl acrylate), which is attributed to the strong UPy-UPy H-bonding interactions. We further conclude that the "effective" adhesion properties of PBA–UPy polymers are determined by the surface density of chains that can interpenetrate across the contacting interface as well as the bulk viscoelasticity of the polymers that determines their viscous forces, both of which are sensitive to humidity and temperature, as illustrated in **Figure 8**.[24,38,46] The presence of UPy functional groups can dramatically enhance the polymer adhesion mainly due to the formation of multiple hydrogen bonds at the contact interface as shown in Figure 8. The adhesion of PBA–UPy polymers also increases dramatically with contact time due to enhanced chain interpenetration and formation of UPy–UPy bonds at (or across) the interface. The PBA–UPy polymers show excellent self-healing ability after the two surfaces are separated and then brought back to contact multiple times, which is attributed to the reversibility, stability, long lifetime and strength of UPy–UPy bonds.[18] Interesting surface deformations and fracture patterns were observed during the separation of PBA–UPy surfaces from adhesive contact. The viscous fingering patterns for PBA–UPy films at relatively high temperature and high humidity level could be well described by the Saffman-Taylor instability theory for viscous failure/rupture. Highly self-organized parellel stripe patterns were obtained for PBA–UPy films at relatively low temperature and low humidity level when the polymers behave more elastically, which may be useful in fabricating patterned surfaces with various applications in materials science and nanotechnology. Our results provide new insights into the fundamental understanding of the adhesive mechanisms of multiple hydrogen-bonding polymers and development of novel self-healing and stimuli-responsive materials.

Supporting Information

Supporting Information is available from the Wiley Online Library or from the author.

Acknowledgement

This work was supported by a Discovery Grant and a RTI Grant from the Natural Sciences and Engineering Research Council of Canada (NSERC) and the Canada Foundation for Innovation (CFI) (H.Z.), the MRSEC Program of the National Science Foundation under Award DMR11–21053 (K.E.F., E.J.K., J.I., and C.J.H.), and the US Department of Energy, Office of Basic Energy Sciences, Division of Materials Sciences under Award DE-FG02–87ER-45331 (J.N.I., experimental planning/design and SFA measurements and interpretation of the results).

Received: August 29, 2013
Revised: October 28, 2013
Published online: January 10, 2014

[1] T. Annable, R. Buscall, R. Ettelaie, *Colloids Surf., A* **1996**, *112*, 97–116.
[2] K. C. Tam, R. D. Jenkins, M. A. Winnik, D. R. Bassett, *Macromolecules* **1998**, *31*, 4149–4159.
[3] R. P. Sijbesma, F. H. Beijer, L. Brunsveld, B. J. B. Folmer, J. J. K. K. Hirschberg, R. F. M. Lange, J. K. L. Lowe, E. W. Meijer, *Science* **1997**, *278*, 1601–1604.
[4] S. Sivakova, D. A. Bohnsack, M. E. Mackay, P. Suwanmala, S. J. Rowan, *J. Am. Chem. Soc.* **2005**, *127*, 18202–18211.
[5] P. Cordier, F. Tournilhac, C. Soulie-Ziakovic, L. Leibler, *Nature* **2008**, *451*, 977–980.
[6] D. Montarnal, F. Tournilhac, M. Hidalgo, J. Couturier, L. Leibler, *J. Am. Chem. Soc.* **2009**, *131*, 7966–7967.
[7] a)K. E. Feldman, M. J. Kade, E. W. Meijer, C. J. Hawker, E. J. Kramer, *Macromolecules* **2009**, *42*, 9072–9081; b) K. E. Feldman, M. J. Kade, E. W. Meijer, C. J. Hawker, E. J. Kramer, *Macromolecules* **2010**, *43*, 5121–5127.
[8] K. E. Feldman, M. J. Kade, T. F. A. de Greef, E. W. Meijer, E. J. Kramer, C. J. Hawker, *Macromolecules* **2008**, *41*, 4694–4700.

[9] J. B. Beck, S. J. Rowan, *J. Am. Chem. Soc.* **2003**, *125*, 13922–13923.
[10] W. Weng, J. B. Beck, A. M. Jamieson, S. J. Rowan, *J. Am. Chem. Soc.* **2006**, *128*, 11663–11672.
[11] H. Zeng, D. S. Hwang, J. N. Israelachvili, J. H. Waite, *Proc. Natl. Acad. Sci. U. S. A.* **2010**, *107*, 12850–12853.
[12] A. Eisenberg, B. Hird, R. B. Moore, *Macromolecules* **1990**, *23*, 4098–4107.
[13] S. I. Stupp, V. LeBonheur, K. Walker, L. S. Li, K. E. Huggins, M. Keser, A. Amstutz, *Science* **1997**, *276*, 384–389.
[14] A. M. Kumar, S. Sivakova, R. E. Marchant, S. J. Rowan, *Small* **2007**, *3*, 783–787.
[15] L. Bouteiller, *Adv. Polym. Sci.* **2007**, *207*, 79–112.
[16] M. M. Caruso, D. A. Davis, Q. Shen, S. A. Odom, N. R. Sottos, S. R. White, J. S. Moore, *Chem. Rev.* **2009**, *109*, 5755–5798.
[17] T. F. De Greef, M. M. Smulders, M. Wolffs, A. P. Schenning, R. P. Sijbesma, E. W. Meijer, *Chem. Rev.* **2009**, *109*, 5687–5754.
[18] T. F. de Greef, E. W. Meijer, *Nature* **2008**, *453*, 171–173.
[19] E. B. Murphy, F. Wudl, *Prog. Poly. Sci.* **2010**, *35*, 223–251.
[20] P. Y. W. Dankers, Z. Zhang, E. Wisse, D. W. Grijpma, R. P. Sijbesma, J. Feijen, E. W. Meijer, *Macromolecules* **2006**, *39*, 8763–8771.
[21] D. J. M. van Beek, A. J. H. Spiering, G. W. M. Peters, K. Nijenhuis, R. P. Sijbesma, *Macromolecules* **2007**, *40*, 8464–8475.
[22] N. Maeda, N. Chen, M. Tirrell, J. N. Israelachvili, *Science* **2002**, *297*, 379–382.
[23] N. Chen, N. Maeda, M. Tirrell, J. Israelachvili, *Macromolecules* **2005**, *38*, 3491–3503.
[24] H. Zeng, N. Maeda, N. Chen, M. Tirrell, J. Israelachvili, *Macromolecules* **2006**, *39*, 2350–2363.
[25] H. Zeng, Y. Tian, B. Zhao, M. Tirrell, J. Israelachvili, *Macromolecules* **2007**, *40*, 8409–8422.
[26] H. Zeng, B. Zhao, Y. Tian, M. Tirrell, L. Gary Leala, J. N. Israelachvili, *Soft Matter* **2007**, *3*, 88–93.
[27] H. Zeng, Y. Tian, B. Zhao, M. Tirrell, J. Israelachvili, *Langmuir* **2007**, *23*, 6126–6135.
[28] H. Zeng, B. Zhao, J. N. Israelachvili, M. Tirrell, *Macromolecules* **2010**, *43*, 538–542.
[29] J. N. Israelachvili, *Intermolecular and Surface Forces* 3rd edn., Academic Press, San Diego, CA, USA **2011**.
[30] D. Leckband, J. Israelachvili, *Q. Rev. Biophys.* **2001**, *34*, 105–267.
[31] J. N. Israelachvili, *J. Colloid Interface Sci.* **1973**, *44*, 259–272.
[32] C. J. van Oss, M. K. Chaudhury, R. J. Good, *Adv. Colloid Interface Sci.* **1987**, *28*, 35–64.
[33] J. N. Israelachvili, P. M. McGuiggan, *J. Mater. Res.* **1990**, *5*, 2223–2231.
[34] J. Israelachvili, Y. Min, M. Akbulut, A. Alig, G. Carver, W. Greene, K. Kristiansen, E. Meyer, N. Pesika, K. Rosenberg, H. Zeng, *Rep. Prog. Phys.* **2010**, *73*, 1–16.
[35] H. Zeng, Y. Tian, T. H. Anderson, M. Tirrell, J. N. Israelachvili, *Langmuir* **2008**, *24*, 1173–1182.
[36] A. Faghihnejad, H. Zeng, *Soft Matter* **2012**, *8*, 2746–2759.
[37] F. Teng, H. Zeng, Q. Liu, *J. Phys. Chem. C* **2011**, *115*, 17485–17494.
[38] (Ed: H. Zeng) *Polymer adhesion, friction and lubrication* John Wiley & Sons, Hoboken, NJ, USA **2013**.
[39] D. Ahn, K. R. Shull, *Langmuir* **1998**, *14*, 3646–3654.
[40] D. Ahn, K. R. Shull, *Langmuir* **1998**, *14*, 3637–3645.
[41] R. G. Horn, J. N. Israelachvili, F. Pribac, *J. Colloid Interface Sci.* **1987**, *115*, 480–492.
[42] H. R. Hertz, *Miscellaneous Papers* **1896**, 340.
[43] K. L. Johnson, K. Kendall, A. D. Roberts, *Proc. R. Soc. London, Ser. A* **1971**, *324*, 301–313.
[44] B. V. Derjaguin, V. M. Muller, Y. P. Toporov, *J. Colloid Interface Sci.* **1975**, *53*, 314–326.
[45] D. Maugis, *J. Colloid Interface Sci.* **1992**, *150*, 243–269.
[46] H. Zeng, M. Tirrell, J. Israelachvili, *J. Adhes.* **2006**, *82*, 933–943.
[47] J. Brandrup, E. H. Immergut, E. A. Grulke, A. Abe, D. R. Bloch, *Polymer Handbook* 4th ed., John Wiley & Sons, New York, USA **2005**.
[48] H. Sun, H. H. Lee, I. Blakey, B. Dargaville, T. V. Chirila, A. K. Whittaker, S. C. Smith, *J. Phys. Chem. B* **2011**, *115*, 11053–11062.
[49] R. M. Barrer, E. K. Rideal, *Trans. Faraday Soc.* **1939**, *35*, 628–643.
[50] G. J. Van Amerongen, *J. Polym. Sci.* **1950**, *5*, 307–332.
[51] S. Prager, F. A. Long, *J. Am. Chem. Soc.* **1951**, *73*, 4072–4075.
[52] P. Meares, *J. Am. Chem. Soc.* **1954**, *76*, 3415–3422.
[53] A. S. Michaels, R. B. Parker, *J. Polym. Sci.* **1959**, *41*, 53–71.
[54] K. E. Feldman, *PhD thesis*, University of California, Santa Barbara **2009**.
[55] K. Kendall, *Science* **1994**, *263*, 1720–1725.
[56] C.-Y. Hui, J. M. Baney, E. J. Kramer, *Langmuir* **1998**, *14*, 6570–6578.
[57] M. O. Robbins, D. Andelman, J. F. Joanny, *Phys. Rev. A* **1991**, *43*, 4344–4354.
[58] E. Barthel, G. Haiat, *Langmuir* **2002**, *18*, 9362–9370.
[59] B. Q. Luan, M. O. Robbins, *Nature* **2005**, *435*, 929–932.
[60] J. A. Greenwood, K. L. Johnson, *J. Colloid Interface Sci.* **2006**, *296*, 284–291.
[61] L. Leger, J. F. Joanny, *Rep. Prog. Phys.* **1992**, *55*, 431–486.
[62] C. Creton, E. J. Kramer, H. R. Brown, C. Y. Hui, *Adv. Polym. Sci.* **2002**, *156*, 53–136.
[63] H. Zeng, Y. Tian, B. X. Zhao, M. Tirrell, J. Israelachvili, *Langmuir* **2009**, *25*, 4954–4964.
[64] L. F. Pease, P. Deshpande, Y. Wang, W. B. Russel, S. Y. Chou, *Nat. Nanotechnol.* **2007**, *2*, 545–548.
[65] J. Nase, A. Lindner, C. Creton, *Phys. Rev. Lett.* **2008**, *101*, 074503.
[66] P. G. Saffman, G. Taylor, *Proc. R. Soc. London, Ser. A* **1958**, *245*, 312–329.
[67] V. Shenoy, A. Sharma, *Phys. Rev. Lett.* **2001**, *86*, 119–122.
[68] A. Ghatak, M. K. Chaudhury, *Langmuir* **2003**, *19*, 2621–2631.
[69] C. J. van Oss, *Interfacial forces in aqueous media* Taylor & Francis, Boca Raton, FL, USA **2006**.